

# ***Comparison of Empirical and Theoretical Computations of Velocity for a Cold Spray Nozzle***

Victor K. Champagne  
Team Leader, Advanced Materials & Processing Team  
US Army Research Laboratory  
vchampag@arl.army.mil

Dennis J. Helfritch  
Scientist, Advanced Materials & Processing Team  
Dynamic Science, Inc.  
dhelfritch@arl.army.mil

Surya Dinavahi  
Onsite CFD Lead at ARL MSRC  
University of Alabama at Birmingham, AL  
dinavahi@uab.edu

**DISTRIBUTION STATEMENT A. Approved for public release; distribution is unlimited.**

## **Abstract**

Cold spray is a process whereby micron-size particles are accelerated to high velocity through entrainment in a gas undergoing expansion in a rocket nozzle and are subsequently impacted upon a surface. The impacted particles, which can be combinations of metals, ceramics and polymeric materials form a consolidated structure which can be several centimeters thick. The characteristics of this structure depend on the initial characteristics of the metal powder and upon the impact velocity.

Two dimensional axi-symmetric computations of the flow through a converging diverging nozzle were performed using the Reynolds Averaged Navier Stokes (RANS) code, CFD++, on ARL MSRC computers. Aluminum particles of constant diameter were injected at the entrance of a De Laval converging, diverging nozzle. The Eulerian Disperse Phase (EDP) capability in CFD++ was used for these simulations. The EDP model couples the dispersed phase with the fluid dynamics. In addition, 1-D, isentropic, gasdynamic equations were solved for the same geometry and initial conditions. The results from the RANS computations and 1-D calculations compared favorably, considering the difference in governing equations.

## **Introduction**

The U.S. Army utilizes metal coatings in many of its weapons systems for the strengthening or protection of vulnerable substrates. The quality of these coatings is characterized by the density of the metal coating and its ability to adhere to the substrate. Extremely dense and adherent metal coatings can be applied to surfaces by impacting metal particles onto the surface at supersonic

velocities. This cold spray process is carried out at the U.S. Army Research Laboratory Center for Cold Spray in Aberdeen, MD.

Cold spray as a coating technology was initially developed in the mid-1980s at the Institute for Theoretical and Applied Mechanics of the Siberian Division of the Russian Academy of Science in Novosibirsk<sup>1</sup>. The Russian scientists successfully deposited a wide range of pure metals, metallic alloys, polymers, and composites onto a variety of substrate materials, and they demonstrated that very high coating deposition rates are attainable using the cold spray process. Currently, a variety of cold spray research is being conducted at institutions in the United States, Russia, Germany, and Japan.

The ARL system accelerates micron-sized particles to high velocities by entraining the particles in the flow of a supersonic nozzle. This system is shown in Figure 1. High velocity is necessary for an optimal particle deposition and coating density, and several parameters, including gas conditions, particle characteristics, and nozzle geometry, affect the particle velocity. It has been well established that impacting particles must exceed a “critical velocity” in order to deposit instead of bouncing off. The magnitude of the critical velocity is given by an empirical relationship, which depends on particle material characteristics, such as density, ultimate strength and melting point as well as the particle temperature immediately before impact<sup>2</sup>. The Army has utilized one dimensional, frictionless, gasdynamic calculations in order to predict gas flow velocities for various cold spray operating conditions. Particle velocities are subsequently iteratively calculated by drag forces and gas-particle velocity difference. Since the powders that are sprayed are characterized by a distribution of diameters, the deposition efficiency for the aggregate of particles within the powder can be determined by calculating the velocities and temperatures of many diameter-groupings and comparing the velocity of each group with the calculated critical velocity for the material<sup>3</sup>.

A concern has centered about the magnitude of overestimation of deposition efficiency due to the neglect of friction and boundary layer effects in the 1-D calculation. This concern initiated efforts to enhance the modeling through the addition of friction via computational fluid dynamics.

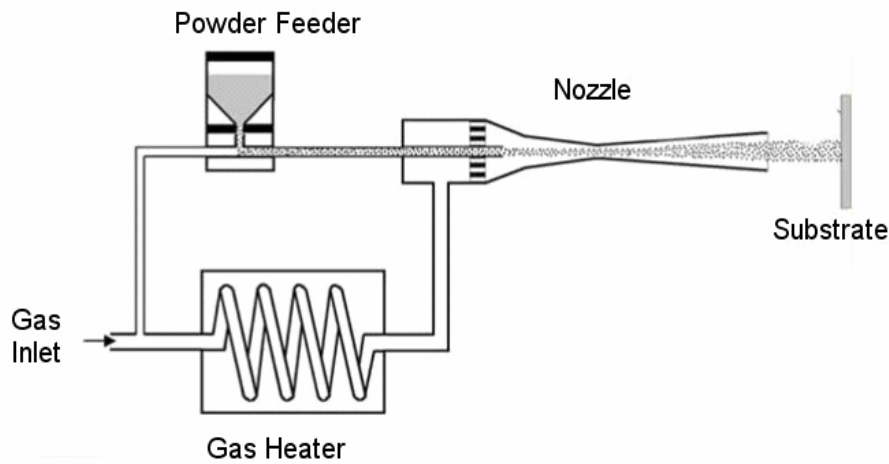


Figure 1. The cold spray process

### Computational Modeling of the Nozzle

The commercially available software, GridPro for generating curvilinear grids and CFD++ for solving the flow are selected for axi-symmetric flow solution. A two dimensional grid is generated using GridPro and the axi-symmetric option is used in CFD++ to simulate the flow through the nozzle. The entire nozzle geometry is shown in Figure 2 to give a general idea of the dimensions involved. The nozzle throat diameter is 2 mm and the exit diameter is 7 mm, for an area ratio of 12.25. The length of the nozzle as modeled is 0.153 m, beginning at the particle injection point and ending at the nozzle exit.

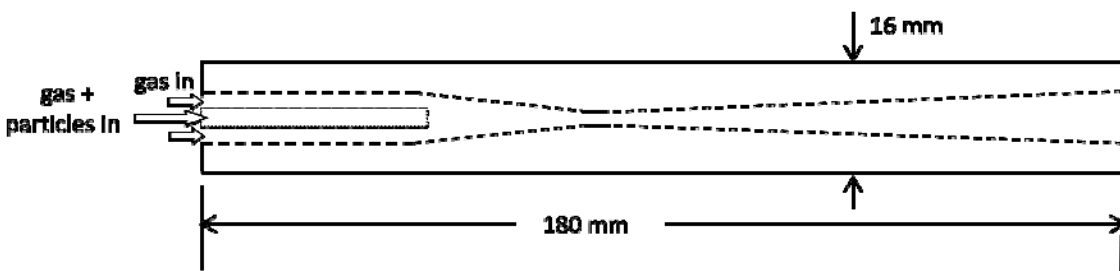


Figure 2. Nozzle geometry (not to scale)

## Problem Setup in CFD++

### Equation Set

We have selected the Reynolds Averaged Navier Stokes (RANS) equation set along with the realizable k-epsilon turbulence model for the fluid. This gives us a total of 6 equations—conservation of mass, conservation of momentum in two dimensions, conservation of energy, an equation for the turbulent kinetic energy,  $k$ , and an equation for turbulence dissipation, epsilon.

CFD++ uses the Eulerian Dispersed Phase (EDP) model to couple the dispersed phase with the fluid dynamics. For the dispersed species, we have an additional three equations to solve. These are the mass equation (eq 1) and the momentum equations in 2 directions (eq 2). In addition to the interphase drag force,  $F_D$ , we have included the effects of pressure gradient force,  $F_{PG}$ , the virtual-mass force,  $F_{VM}$ , lift force,  $F_L$ , and the turbulent dispersion force,  $F_{TD}$ , on the particles. The effect of gravity is not included due to the small particle size (15 e-6 m diameter) and the high speeds (Mach 1-3) involved.

$$\frac{\partial(\rho_{pi})}{\sigma t} + \nabla \cdot (\rho_{pi} \vec{u}_{pi}) = 0 \quad (\text{eq 1})$$

Where  $\rho$  is the gas density and  $u$  is velocity.

$$\frac{\partial(\rho_{pi} \vec{u}_{pi})}{\sigma t} + \nabla \cdot (\rho_{pi} \vec{u}_{pi} \vec{u}_{pi}) = \vec{F}_{D_i} + \vec{F}_{VM_i} + \vec{F}_{TD_i} + \vec{F}_{L_i} + \vec{F}_{PG_i} \quad (\text{eq 2})$$

### Computational Grid

The computational grid in and around the nozzle is shown in Figure 3. The half-plane of the full nozzle is shown, followed by the grid near the end of the inner tube at the beginning of the converging section and the grid near the exit of the nozzle. The grid spacing in the wall normal direction is 1e-6 m and in the direction normal to the axis is 1e-5 m.

### Boundary Conditions

At the annulus inlet, the static pressure and temperature are set to 3.2e6 Pa and 673.15 K respectively. At inner injection tube, the static pressure of 3.2e6 Pa and a temperature of 293.15 K are applied. The aluminum particles are assumed to be spherical, of 15E-6 m diameter. Also the fluidized density of the aluminum is set at 10 kg/m<sup>3</sup> at the inlet of the inner injection tube. All the walls are treated as viscous adiabatic. At the two outer boundaries, the room pressure and temperature are applied. Also, at these boundaries the flow is allowed to flow in either direction. This boundary condition is referred to in CFD++ as “Pres. Temp. inflow/outflow using inside velocity.” The boundary conditions are summarized in the Table 1 below. These boundary conditions lead to the calculated mass flow rates of N2 of 1.4e-2 kg/s through the annulus and 4e-3 kg/s through the inner tube. The computed mass flow rate of Al through the inner tube is

7.6e-4 kg/s. A free-stream distance of 25E-3m is assumed between the nozzle exit and an impact plane.

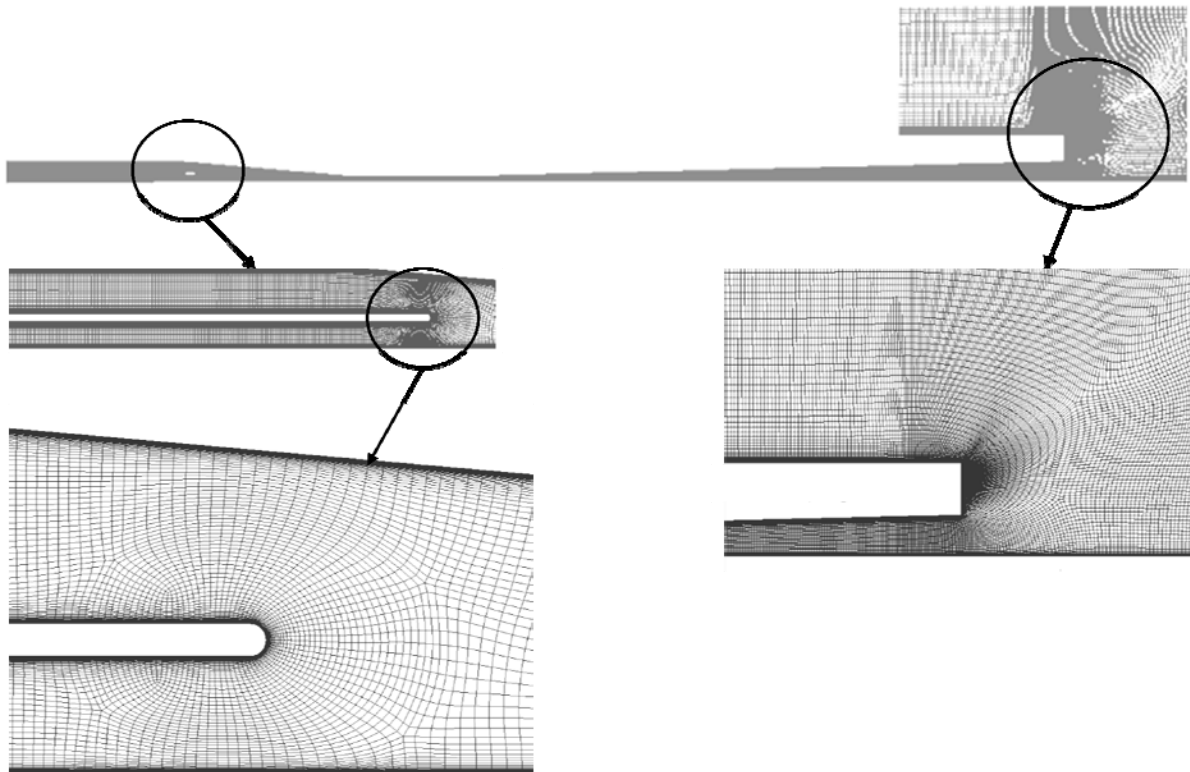


Figure 3. The grid construction.

Table 1 Boundary conditions

	P (Pa)	T (K)	Density	Velocity
Inlet Annulus	3.2E-6	693.15	-	-
Inlet Inner tube	3.2E06	293.15	Al 10 Kg/m <sup>3</sup>	-
Nozzle Wall	-	Adiabatic	-	Viscous.
Inner Tube Wall	-	Adiabatic	-	Viscous
Substrate/Far Wall	-	Adiabatic	-	Viscous
Top Exit	101325	293.15	-	-
Left Exit	101325	293.15	-	-

## One-Dimensional Model

The modeling of particle velocity is carried out in two steps:

1. The gas flow and temperature in the nozzle are calculated by means of isentropic gas dynamic principles.
2. Friction between gas and particles is subsequently introduced as a drag coefficient is used to iteratively calculate particle velocity through the nozzle.

### Gas Flow

The gas flow model uses isentropic relationships and linear nozzle geometry. The assumptions for the calculation are as follows:

- The gas flow is inviscid.
- The gas flow is adiabatic, i.e., no heat loss occurs to the surroundings.
- Flow through the nozzle is one-dimensional; hence, the flow velocity, pressure, and density are uniform across any cross section normal to the nozzle axis.
- Particles do not influence gas conditions.

Under these conditions, the relationship between the nozzle area,  $A$ , and the Mach number is given by Equation 3, where  $\gamma$  is the ratio of gas specific heats ( $C_p/C_v$ ):

$$\frac{A_1}{A_2} = \frac{M_2}{M_1} \left\{ \frac{1 + [(\gamma - 1)/2]M_1^2}{1 + [(\gamma - 1)/2]M_2^2} \right\}^{\frac{(\gamma+1)}{2(\gamma-1)}} \quad (\text{Eq 3})$$

Since the 1-D computation depends only on flow area, the simple, conical nozzle geometry shown in Figure 4 is assumed.

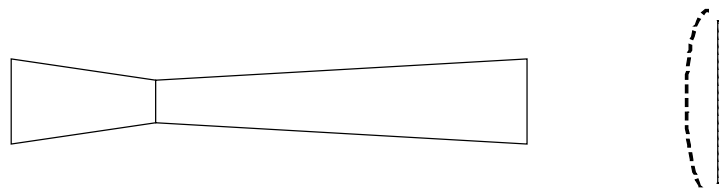


Figure 4. Nozzle-shock wave-substrate geometry.

A small initial subsonic Mach number and initial (stagnation) values of pressure and temperature are assigned at the converging section of the nozzle. The Mach number is then iteratively increased, while gas characteristics are calculated for each point through the isentropic

relationships of Equations 4 and 5. Linear progression along the nozzle axis is calculated from the area change given by Equation 1 and the assumed nozzle geometry.

$$\frac{T_0}{T} = 1 + \left( \frac{\gamma - 1}{2} \right) M^2 \quad (\text{Eq 4})$$

$$\frac{p_0}{p} = \left[ 1 + \left( \frac{\gamma - 1}{2} \right) M^2 \right]^{\frac{\gamma}{\gamma - 1}} \quad (\text{Eq 5})$$

The flow between the nozzle exit and the shock wave upstream of the substrate is assumed to be constant, and equal to the conditions at the nozzle exit. The stand-off position of the shock wave relative to the substrate is given by Billig's approximation<sup>4</sup> as:

$$\Delta = 0.143d_e \left[ \exp \left( 3.24 / M_e^2 \right) \right] \quad (\text{Eq 6})$$

where  $d_e$  equals the nozzle exit diameter, and  $M_e$  is the Mach number at the nozzle exit.

The Mach number immediately behind the shock wave is given by the normal shock relationship:

$$M^2 = \frac{\left[ M_e^2 + \frac{2}{\gamma - 1} \right]}{\left[ \left( \frac{2\gamma}{\gamma - 1} \right) M_e^2 - 1 \right]} \quad (\text{Eq 7})$$

### Particle Motion

Once the gas conditions and velocity are characterized, the particle velocity is iteratively calculated from the nozzle entrance to the substrate through the use of a solid rocket nozzle particle drag relationship. This relationship predicts the accelerating force on the particle:

$$m \frac{dV_p}{dt} = C_D (\pi / 8) \rho_g d^2 (V_g - V_p)^2 \quad (\text{Eq 8})$$

$V_p$  and  $V_g$  are particle and gas velocities,  $m$  is the particle mass,  $\rho_g$  is the gas density, and  $d$  is the particle diameter.

Carlson and Hoglund<sup>5</sup> correct the simple Stokes drag law relationship for inertial, compressibility, and rarefaction effects through the empirical relationship of Equation 9:

$$C_D = \frac{24}{R_e} \left[ \frac{\left(1 + 0.15R_e^{0.687}\right) \left(1 + e^{-0.427/M_p^{4.63} + 3.0/R_e^{0.88}}\right)}{1 + \left(M_p / R_e\right) \left(3.82 + 1.28e^{-1.25R_e/M_p}\right)} \right] \quad (\text{Eq 9})$$

where  $M_p$  is the Mach number of the gas-particle velocity difference and  $R_e$  is the gas-particle Reynolds number.

### 1-D Boundary and Initial Conditions

The nozzle shape, ie radius versus distance from the inlet, was chosen to be equal to that used for the CFD computation. The stagnation pressure is assumed to be 3.2E6 Pa as given by Table 1. The stagnation temperature is assumed to be 588 K, which corresponds to the mixed temperature of the inlet annulus and inlet inner tube of Table 1. The aluminum particle characteristics are equal to that of the CFD computation.

### Comparative Results

The velocity results of the CFD and 1-D computations are shown in Figure 5. The CFD contour visualizations show flow separation near the nozzle exit, due to the overexpanded area ratio of the nozzle. A series of shock/expansion waves follow nozzle exit. The longitudinal velocity approaches zero at the boundary wall. Radial velocity is not shown in this figure, so gas deflection at the wall is not visualized.

Particles are uniformly accelerated by the gas flow. They are relatively unaffected by the extreme variations in gas velocity at the nozzle exit, due to the momentum of the particles. Unlike the gas, the longitudinal particle velocity remains high to the point of boundary impact.

The 1-D results, as well as the axial CFD computed velocities are shown in the graph, where the x scale corresponds to the nozzle visualizations above. The 1-D computation yields velocities that are approximately 100 m/s higher than that of the CFD computation. This difference can be attributed to the inviscid assumption of the 1-D calculation. Additionally, the 1-D calculation does not take the transition between nozzle wall and free space into account.

### Conclusions

The similarity in results of the CFD and 1-D computations is good, considering that the equation sets utilized for calculation are significantly different. The CFD computation clearly results in more flow field information and includes viscous effects, such as boundary layer. This frictional effect leads to a slightly lower gas velocity when compared to inviscid 1-D.

The computations show particle impact velocities above 650 m/s. ARL has shown that aluminum deposition results when operating the given nozzle at the initial conditions chosen for these computations. It is also known that velocities below approximately 600 m/s do not result in aluminum deposition<sup>2</sup>. The computational results are thus verified by known cold spray performance. These computational techniques are currently applied for feasibility to new cold spray applications.

### Future Work

Experiments are planned to measure the particle velocities using LASER velocimetry at several down stream locations between the nozzle exit and the substrate. The obtained measurements will be compared with those from the calculations.

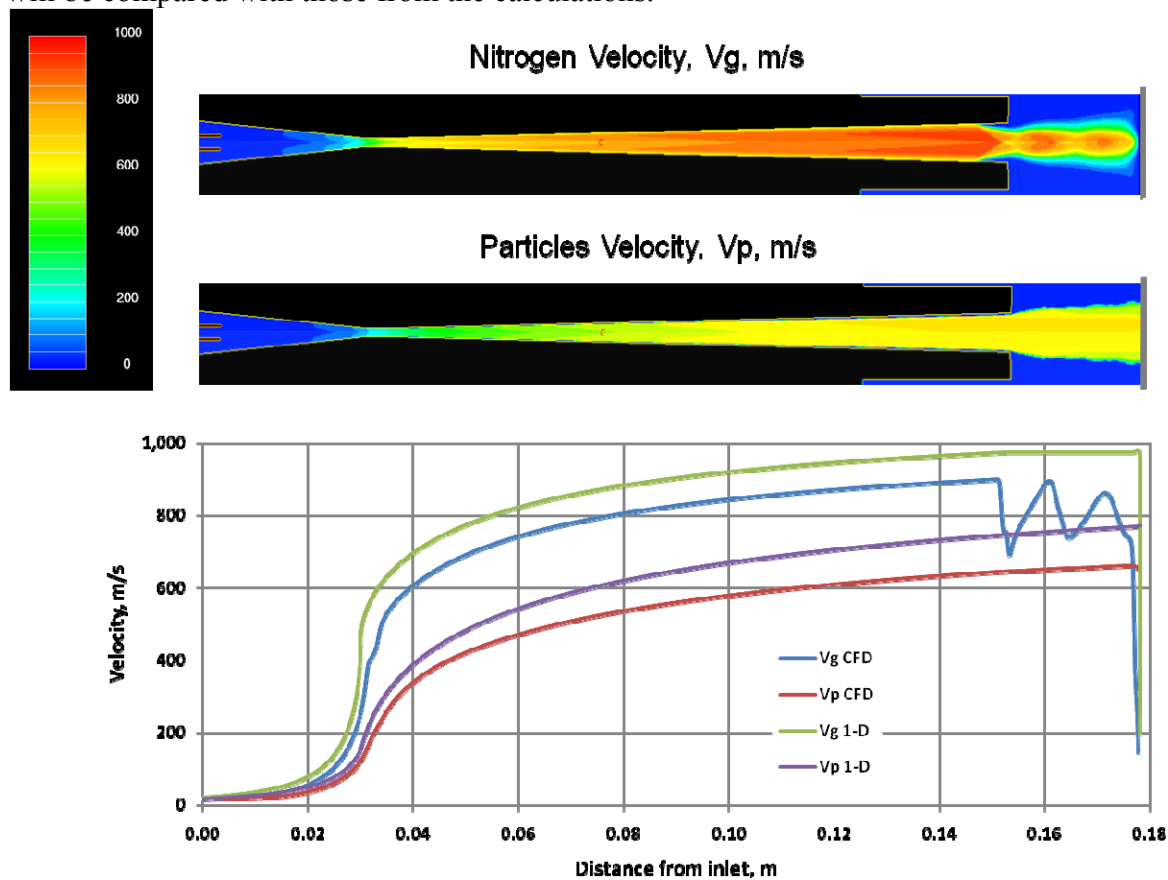


Figure 5. Velocity results.

### Acknowledgements

Computer resources were provided by the U.S. Department of Defense, High Performance Computing, Major Shared Resource Center at ARL APG. The work of Surya Dinavahi is made possible through support provided by DoD HPCMP PET activities through Mississippi State University under contract No. GS04T01BFC0060. Surya Dinavahi also acknowledges the

support of the University of Alabama at Birmingham. We thank Dr Nili Bachchan at Metacomp Technologies, Inc for helping us to get up to speed with EDP technology in CFD++.

## References

1. A. Papyrin, Cold Spray Technology, *Adv. Mater. Process.*, Sept. 2001, p. 49–51.
2. T. Schmidt, et al, Development of a generalized parameter window for cold spray deposition, *Acta Materialia*, Vol 54, 2006, pp 729 - 742.
3. V. Champagne, et al, The effects of gas and metal characteristics on sprayed metal coatings, *Modelling Simul. Mater. Sci. Eng.* Vol 13, 2005, pp. 1–10
4. F.S. Billig, Shock-Wave Shapes around Spherical and Cylindrical-Nosed Bodies, *J. Spacecraft*, Vol. 4(No. 5), 1967, pp. 822 - 823.
5. D. Carlson and R. Høglund, Particle Drag and Heat Transfer in Rocket Nozzles, *AIAA Journal*, Vol 2 (No. 11), 1964, pp. 1980 -1984.